Ann. Geophys., 31, 1653–1671, 2013
www.ann-geophys.net/31/1653/2013/
doi:10.5194/angeo-31-1653-2013

Annales Geophysicae
Open Access

Empirical regional models for the short-term forecast of *M3000F2* during not quiet geomagnetic conditions over Europe

M. Pietrella

Istituto Nazionale di Geofisica e Vulcanologia, via di Vigna Murata 605, 00143 Rome, Italy

Correspondence to: M. Pietrella (marco.pietrella@ingv.it)

Received: 14 May 2013 – Revised: 29 July 2013 – Accepted: 31 July 2013 – Published: 7 October 2013

Abstract. Twelve empirical local models have been developed for the long-term prediction of the ionospheric characteristic *M3000F2*, and then used as starting point for the development of a short-term forecasting empirical regional model of *M3000F2* under not quiet geomagnetic conditions. Under the assumption that the monthly median measurements of *M3000F2* are linearly correlated to the solar activity, a set of regression coefficients were calculated over 12 months and 24 h for each of 12 ionospheric observatories located in the European area, and then used for the long-term prediction of *M3000F2* at each station under consideration.

Based on the 12 long-term prediction empirical local models of *M3000F2*, an empirical regional model for the prediction of the monthly median field of *M3000F2* over Europe (indicated as *RM_M3000F2*) was developed.

Thanks to the *IFELM_foF2* models, which are able to provide short-term forecasts of the critical frequency of the F2 layer ($foF2_{STF}$) up to three hours in advance, it was possible to considerer the Brudley–Dudeney algorithm as a function of $foF2_{STF}$ to correct *RM_M3000F2* and thus obtain an empirical regional model for the short-term forecasting of *M3000F2* (indicated as *RM_M3000F2_BD*) up to three hours in advance under not quiet geomagnetic conditions.

From the long-term predictions of *M3000F2* provided by the IRI model, an empirical regional model for the forecast of the monthly median field of *M3000F2* over Europe (indicated as *IRI_RM_M3000F2*) was derived.

IRI_RM_M3000F2 predictions were modified with the Bradley–Dudeney correction factor, and another empirical regional model for the short-term forecasting of *M3000F2* (indicated as *IRI_RM_M3000F2_BD*) up to three hours ahead under not quiet geomagnetic conditions was obtained.

The main results achieved comparing the performance of *RM_M3000F2*, *RM_M3000F2_BD*, *IRI_RM_M3000F2*, and *IRI_RM_M3000F2_BD* are (1) in the case of moderate geomagnetic activity, the Bradley–Dudeney correction factor does not improve significantly the predictions; (2) under disturbed geomagnetic conditions, the Bradley–Dudeney formula improves the predictions of *RM_M3000F2* in the entire European area; (3) in the case of very disturbed geomagnetic conditions, the Bradley–Dudeney algorithm is very effective in improving the performance of *IRI_RM_M3000F2*; (4) under moderate geomagnetic conditions, the long-term prediction maps of *M3000F2* generated by *RM_M3000F2* can be considered as short-term forecasting maps providing very satisfactory results because quiet geomagnetic conditions are not so diverse from moderate geomagnetic conditions; (5) the forecasting maps originated by *RM_M3000F2*, *RM_M3000F2_BD*, and *IRI_RM_M3000F2_BD* show some regions where the forecasts are not satisfactory, but also wide sectors where the *M3000F2* forecasts quite faithfully match the *M3000F2* observations, and therefore *RM_M3000F2*, *RM_M3000F2_BD*, and *IRI_RM_M3000F2_BD* could be exploited to produce short-term forecasting maps of *M3000F2* over Europe up to 3 h in advance.

Keywords. Ionosphere (ionosphere–magnetosphere interactions; ionospheric disturbances; modelling and forecasting)

1 Introduction

Ionospheric models providing a full specification of the three-dimensional (3-D) electron density profile are very important because they can be considered as an essential starting point to carry out a lot of other research (Bilitza, 2002; Cander, 2008). Recently the ISP model capable of providing a 3-D electron density profile representation of the

ionosphere in real time for quiet and disturbed geomagnetic conditions (Pezzopane et al., 2011, 2013) was developed and then used for calculating a 3-D ray tracing in the ionospheric medium on the base of measured oblique ionograms over a given radio link (Settimi et al., 2013).

Moreover, the development of models that are able to provide reliable predictions of the most important ionospheric characteristics is very important to ensure successful radio communications. For this reason, many global models, such as the International Reference Ionosphere (IRI) (Bilitza, 2001; Bilitza and Reinisch, 2008) and NeQuick (Radicella, 2009), and regional models (Zolesi et al., 1993, 1996; De Franceschi et al., 2000; Bradley, 1999; Hanbaba, 1999) have been developed over the years to predict the monthly medians of the main ionospheric parameters such as the highest frequency reflected by the F2 layer, (*fo*F2), and the secant of the optimum angle at which to broadcast a signal that is to be received at a distance of 3000 km (*M(3000)F2*).

Several different techniques have been developed for forecasting the ionospheric characteristics. Artificial neural networks (Francis et al., 2001; Cander et al., 2003; Chen et al., 2008), the multiple linear regression method (Mikhailov et al., 1999), the autocorrelation method (Liu et al., 2005), and autoregression method (Koutroumbas et al., 2008) are some of the techniques available to forecast the ionospheric parameters significant for purposes of radio communication. These techniques give reliable predictions essentially for a quiet ionosphere, but they are not successful in the case of disturbed ionospheric conditions (Cander, 2003). A high degree of reliability during quiet ionospheric conditions is also provided by the two global climatological models IPS-ASAPS (IPS-Radio and Space Services, 2013) and ICEPAC (Stewart, 2013), capable of offering good guidelines for the selection of maximum usable frequencies to be used for radio communications for not disturbed ionospheric conditions (Zolesi et al., 2008), but they fail when disturbed ionospheric situations associated with geomagnetic storm events occur (Pietrella et al., 2009).

During magneto-ionospheric storms events considerable variations can occur in electron density content altering day-to-day F region ionospheric variability so that the long-term prediction models for *fo*F2 and *M3000F2* are not able to supply reliable forecasts.

For this reason arises the necessity to develop short-term forecasting models (Cander et al., 1998; Muhtarov and Kutiev, 1999; Stanislawska and Zbyszynski, 2002; Oyeyemi et al., 2005; Pietrella and Perrone, 2008; Strangeways et al., 2009), able to provide predictions of *fo*F2 and *M3000F2* a few hours in advance, and nowcasting models (Araujo-Pradere et al., 2002; Zolesi et al., 2004; Tsagouri et al., 2005; Pietrella and Perrone, 2005; Pietrella et al., 2009), to obtain forecasts of the ionospheric parameters in quasi real time.

The use of these models would provide HF operators with real-time or quasi-real-time support in selecting the best possible frequencies in order to guarantee an efficient maintenance of radio links, also in the case of not quiet magneto-ionospheric conditions.

Table 1. List of ionospheric observatories used for the development of the short-term forecasting procedures: the interval of years for which the monthly median measurements are taken into account to calculate the set of regression coefficients (column A) and the interval of years considered to test the reliability of the models (column B) are shown for all the stations.

MLS	Latitude	Longitude	A	B
Tortosa	40°8′ N	0°5′ E	1955–1986	1987–2001
Rome	41°8′ N	12°5′ E	1957–1990	1991–2000
Poitiers	46°6′ N	0°3′ E	1957–1988	1989–1998
Lannion	48°1′ N	2°3′ E	1961–1987	1988–1997
MHLS	Latitude	Longitude	A	B
Dourbes	50°1′ N	4°6′ E	1957–1987	1988–1997
Slough	51°5′ N	−0°6′ W	1957–1989	1990–2003
Juliusruh	54°6′ N	13°4′ E	1957–1990	1991–2003
Kaliningrad	54°7′ N	20°6′ E	1964–1986	1987–1994
Uppsala	59°8′ N	17°6′ E	1957–1988	1989–1998
HLS	Latitude	Longitude	A	B
Lyckesele	64°6′ N	18°8′ E	1957–1987	1988–1998
Sodankyla	67°4′ N	26°6′ E	1957–1987	1988–1997
Kiruna	67°8′ N	20°4′ E	1957–1985	1986–1998

More recently a short-term ionospheric forecasting empirical regional model to predict the critical frequency of the F2 layer (*IFERM_foF2*) during moderate, disturbed and very disturbed geomagnetic conditions over the European area was developed by Pietrella (2012).

When geomagnetic storms occur, the Earth's magnetic field strength varies significantly from place to place. As the intensity of the phenomena observed in the F region of the ionosphere during ionospheric storms is strictly related to the magnetic field strength, the main element for discerning the various effects that a storm has on the behaviour of the F region is the difference in latitude of a place to another one.

This means that *N* local models for the prediction of *M3000F2* adequately scattered in latitude, each of which having the skill to properly capture the local effects of a storm on *M3000F2*, could be used all together at the same time to reproduce the effects of the storm on the F region over a spatial scale larger than the local one.

Consequently, the predictions of *M3000F2* obtained by *N* local models at a given epoch can be suitably utilized to generate forecasting maps of *M3000F2* during geomagnetic storm events over the region comprising the *N* models.

With these considerations in mind, and inspired by the work of Pietrella (2012), two different empirical regional models for the short-term forecasting of *M3000F2* over the European area were derived on the basis of 12 short-term forecasting empirical local models which have been developed following two diverse procedures.

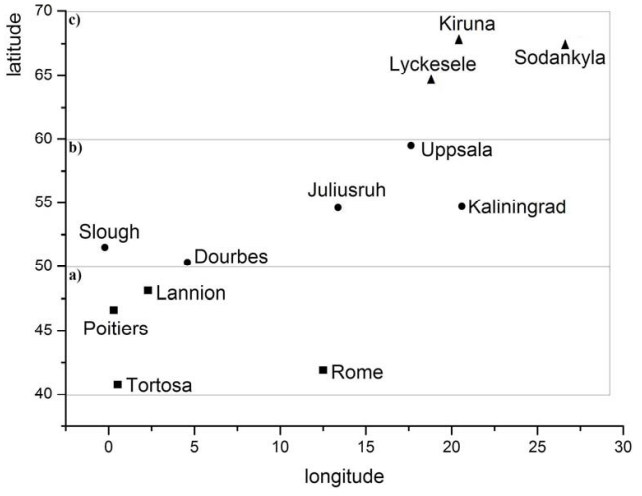

Fig. 1. Geographic area showing the 12 ionospheric observatories for which the short-term forecasting empirical local models were developed. **(a)** The squares mark the stations situated at middle latitudes (40° N $\leq \lambda \leq 50^\circ$ N); **(b)** the circles mark the stations located at middle-high latitudes (50° N $< \lambda \leq 60^\circ$ N); **(c)** the triangles mark the stations placed at high latitudes (60° N $< \lambda \leq 70^\circ$ N).

The 12 local observatories considered for the development of the forecasting procedures are Tortosa, Rome, Poitiers, and Lannion (Fig. 1a); Dourbes, Slough, Juliusruh, Kaliningrad, and Uppsala (Fig. 1b); and Lyckesele, Sodankyla, and Kiruna (Fig. 1c).

The first procedure followed for the achievement of the short-term forecasts of *M3000F2* takes into account the monthly median measurements of *M3000F2*, i.e. those monthly median values that were obtained from the measurements of *M3000F2* recorded at each ionospheric observatory over the years as shown in column A of Table 1.

Using the linear relationship between the 12-month smoothed mean value of the monthly sunspot numbers (R_{12}) and the monthly median measurements of *M3000F2* (see CCIR Report 340-6, 1991), a set of statistically significant regression coefficients were established for each observatory over 12 months and 24 h, and utilized as input to calculate the monthly median predictions of *M3000F2* for each local station. To the monthly median values of *M3000F2* predicted with the long-term prediction models which are discussed below, we refer hereafter also as monthly median field.

Based on these 12 local models providing long-term predictions of *M3000F2*, an empirical regional model for the achievement of the monthly median field of *M3000F2* over the European sector (indicated as *RM_M3000F2*) was also derived. Subsequently the monthly median field of *M3000F2* predicted at each ionospheric observatory was modified by means of the Bradley–Dudeney algorithm (Bradley and Dudeney, 1973), which depends on the critical frequency of the E layer (*fo*E), and the hourly short-term forecasts of *fo*F2 ($foF2_{STF}$), provided by the 12 short-term forecasting empirical local models (*IFELM_foF2*) developed by Pietrella (2012). As $foF2_{STF}$ can be forecasted up to three hours in advance under different geomagnetic conditions, the Bradley–Dudeney correction factor confers characteristics of short-term forecast for *M3000F2*, and therefore its application to the monthly median field of *M3000F2* was used to generate 12 empirical local models for the short-term forecasting of *M3000F2* up to three hours ahead. Based on these 12 short-term forecasting empirical local models, an empirical regional model for the short-term forecasting of *M3000F2* (indicated as *RM_M3000F2_BD*) up to three hours in advance under different geomagnetic conditions was also obtained.

The second procedure followed to obtain *M3000F2* predictions over Europe takes into account the monthly median predictions of *M3000F2* provided by the IRI model at each local station. From these predictions an empirical regional model for the achievement of the IRI monthly median field of *M3000F2* over Europe (indicated as *IRI_RM_M3000F2*) was also implemented. The IRI monthly median field of *M3000F2* was corrected with the Bradley–Dudeney algorithm at each ionospheric observatory to generate 12 empirical local models for the short-term forecasting of *M3000F2* up to three hours ahead. Based on these 12 short-term forecasting empirical local models, an empirical regional model for the short-term forecasting of *M3000F2* (indicated as *IRI_RM_M3000F2_BD*) up to three hours in advance under different geomagnetic conditions was also obtained.

The geomagnetic index used in this study to distinguish the different ranges of geomagnetic activity is the ap(τ) index introduced by Wrenn (1987). Based on previous research (Wrenn et al., 1987; Perrone et al., 2001, and references therein; Pietrella, 2012), many epochs occurring over the years shown in column B of Table 1 were chosen and thereafter classified on the basis of three different ranges of geomagnetic activity: moderate ($7 <$ ap(τ) ≤ 20); disturbed ($20 <$ ap(τ) ≤ 32); and very disturbed (ap(τ) > 32).

Afterwards, these epochs have been grouped together and the predictions of *M3000F2* provided by *RM_M3000F2*, *RM_M3000F2_BD*, *IRI_RM_M3000F2*, and *IRI_RM_M3000F2_BD* were calculated and binned by single month. The hourly measurements of *M3000F2* relative to the epochs selected were taken into account to test the performance of each model for all the months in terms of global root mean square deviation (g.r.m.s.) error under moderate, disturbed, and very disturbed geomagnetic activity.

Some comparisons between the maps based on *M3000F2* measurements and the maps obtained by the forecasts generated by the *RM_M3000F2*, *RM_M3000F2_BD*, and *IRI_RM_M3000F2_BD* models are also presented for a few days characterized by moderate, disturbed, and very disturbed geomagnetic activity.

Section 2 describes the data used and how the models were developed. Section 3 outlines the

testing procedure and illustrates the related comparisons and results. The discussion concerning the *RM_M3000F2/RM_M3000F2_BD/IRI_RM_M3000F2/IRI_RM_M3000F2_BD* approach, as well as some final remarks on possible future developments, is given in Sect. 4.

2 Data used and description of the procedures followed for the achievement of the regional forecasting models of *M3000F2*

As can be seen in Table 1, the 12 ionospheric observatories considered in this study have been separated as follows: Tortosa, Rome, Poitiers, and Lannion located at middle latitudes ($40° \text{ N} \leq \lambda \leq 50° \text{ N}$), hereafter also referred to simply as MLS; Dourbes, Slough, Juliusruh, Kaliningrad, and Uppsala located at middle-high latitudes ($50° \text{ N} < \lambda \leq 60° \text{ N}$), hereafter also referred to simply as MHLS; and Lyckesele, Sodankyla, and Kiruna located at high latitudes ($60° \text{ N} < \lambda \leq 70° \text{ N}$), hereafter also referred to simply as HLS.

The parameters utilized for the achievement of the short-term forecasting models were (a) the monthly median measurements of *M3000F2* acquired in 12 ionospheric observatories over a large period of years (Table 1, column A); (b) the monthly median predictions of *M3000F2*, and the predictions of the critical frequency of the E region (*fo*E) provided by the IRI model at each ionospheric observatory; and (c) the hourly short-term forecasts of *fo*F2 up to 3 h in advance, provided by the 12 short-term forecasting empirical local models (*IFELM_foF2*) developed by Pietrella (2012). In addition, the hourly time-weighted accumulation series derived from the geomagnetic planetary index ap (ap(τ)) were used to select the different ranges of geomagnetic activity.

As regards the first procedure followed for the achievement of a short-term forecasting empirical regional model, as the first step, the linear relationship between the monthly median measurements of *M3000F2* ($M3000F2_{\text{MED,MEAS,s,m,hh}}$), recorded over the years reported in column A of Table 1, and the 12-month smoothed mean value of the monthly sunspot numbers (R_{12}) was considered for each local station:

$$M3000F2_{\text{MED,MEAS,s,m,hh}} = A_{\text{s,m,hh}} + B_{\text{s,m,hh}} \cdot R_{12}, \quad (1)$$

where s, m, and hh indicate the station, month, and hour respectively.

From Eq. (1) a set of 288 (12 months $\times$ 24 h) pairs of statistically significant coefficients ($A^*_{\text{s,m,hh}}$, $B^*_{\text{s,m,hh}}$) were established by means of a linear regression analysis for each observatory, and utilized as input to calculate the monthly median predictions of *M3000F2* at each local station.

Each set of 288 pairs of coefficient represents a model for the prediction of the monthly median values of *M3000F2* ($M3000F2_{\text{MED\_PRED,s,m,hh}}$) for a given local station s, at a well-specified future epoch (year, month, and hour):

$$M3000F2_{\text{MED\_PRED,s,m,hh}} = A^*_{\text{s,m,hh}} + B^*_{\text{s,m,hh}} \cdot R_{12,\text{PREV}}, \quad (2)$$

where $R_{12,\text{PREV}}$ is the 12-month smoothed mean value of the monthly sunspot numbers predicted at the epoch under consideration. As in Eq. (2) the s index varies from 1 to 12; Eq. (2) represents 12 empirical local models providing long-term predictions of *M3000F2*, and as such they can be considered as a single empirical regional model for the long-term prediction of *M3000F2* to which henceforward we refer as *RM_M3000F2*.

$M3000F2_{\text{MED\_PRED,s,m,hh}}$ values predicted by each local model were then modified through the correction factor $\Delta M\_BD_{\text{STF,s,m,d,hh}}$ provided by the empirical formula of Bradley and Dudeney (1973):

$$\Delta M\_BD_{\text{STF,s,m,d,hh}} = \frac{0.18}{\frac{foF2_{\text{STF}_{\text{s,m,d,hh}}}}{foE_{\text{s,m,d,hh}}} - 1.4}, \quad (3)$$

where STF stands for "short-term forecast" and s, m, d, and hh indicate the station, month, day, and hour respectively.

At this point, it is very important to point out that in Eq. (3) correcting the monthly medians predictions of *M3000F2*, the values of the critical frequency of the E layer ($foE_{\text{s,m,d,hh}}$) were obtained by the IRI model, whereas the values of the critical frequency of the F2 layer ($foF2_{\text{STF,s,m,d,hh}}$) are those predicted by the 12 local models developed by Pietrella (2012) providing the short-term forecast of *fo*F2 up to three hours in advance under moderate ($7 < \text{ap}(\tau) \leq 20$), disturbed ($20 < \text{ap}(\tau) \leq 32$), and very disturbed ($\text{ap}(\tau) > 32$) geomagnetic conditions. This means that the Bradley–Dudeney correction factor confers characteristics of short-term forecast for *M3000F2*, and hence its application corrects the predicted monthly median field of *M3000F2* at each local station, thus generating 12 empirical local models providing short-term forecasting of *M3000F2* up to three hours ahead.

Therefore, depending on whether the short-term forecast of *fo*F2 ($foF2_{\text{STF,s,m,d,hh}}$) was acquired in the case of moderate, disturbed, and very disturbed geomagnetic activity, $\Delta M\_BD_{\text{STF,s,m,d,hh}}$ can be seen as the correction factor of the monthly median field of *M3000F2* under moderate, disturbed, and very disturbed geomagnetic conditions respectively, because $foE_{\text{s,m,d,hh}}$ in Eq. (3) is not affected by the magneto-ionospheric storms.

The correction of the predicted monthly median values of *M3000F2* by means of $\Delta M\_BD_{\text{STF,s,m,d,hh}}$,

$$M3000F2_{\text{STF,s,m,d,hh}} = M3000F2_{\text{MED\_PRED,s,m,hh}} + \Delta M\_BD_{\text{STF,s,m,d,hh}}, \quad (4)$$

constitutes a model that is able to provide short-term forecasts of *M3000F2* for each observatory in diverse geomagnetic conditions because the predictions provided by Eq. (4) are connected with the short-term forecasts of *fo*F2. Given that the s index varies from 1 to 12, Eq. (4) represents 12

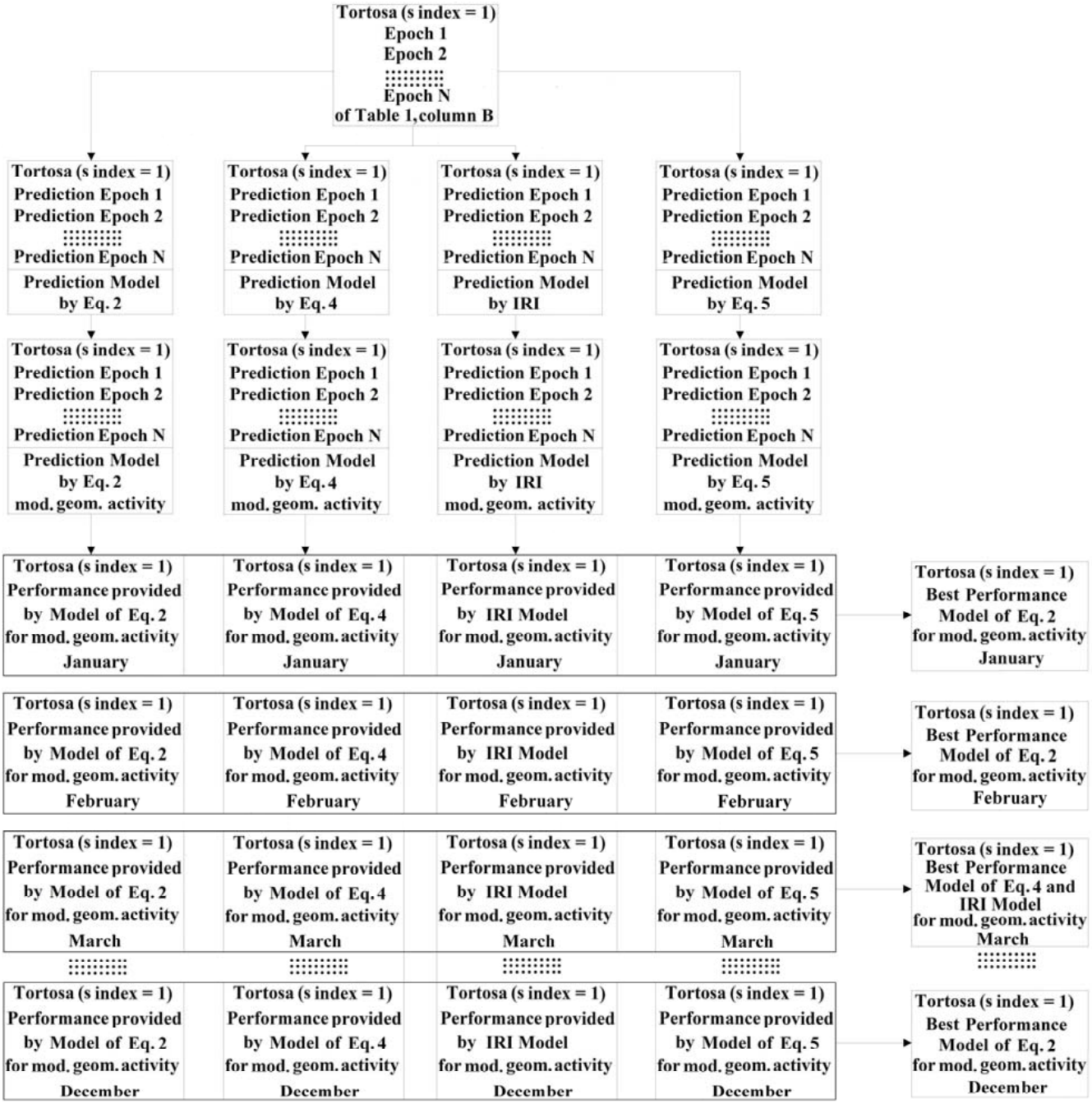

Fig. 2. Example of a flowchart describing the procedure followed to select the forecasting models providing the best performance in Tortosa under moderate geomagnetic conditions.

short-term forecasting empirical local models that all together can be considered as a single short-term forecasting empirical regional model of *M3000F2* to which henceforward we refer as *RM_M3000F2_BD*.

Concerning the second procedure carried out for the achievement of another short-term forecasting empirical regional model, it is based on the predictions of the monthly median values of *M3000F2* provided by the IRI model at each ionospheric observatory. These predictions, indicated as $IRI\_M3000F2_{MED\_PRED,s,m,hh}$ where the s index is ranged between 1 and 12, constitute all together a single empirical regional model for the long-term prediction of *M3000F2* to which henceforward we refer as *IRI_RM_M3000F2*.

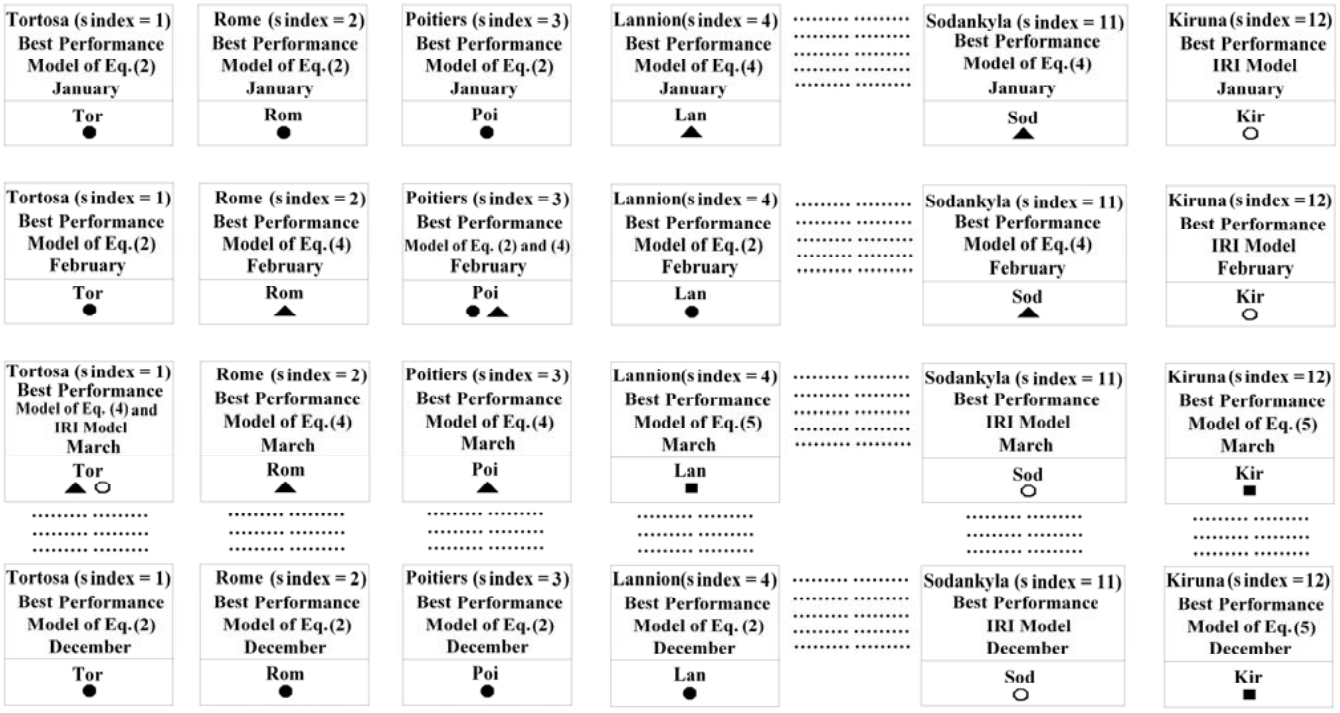

Fig. 3. Example of models providing the best performance (marked with a different symbol) for some ionospheric observatories and for some months, under moderate geomagnetic conditions.

The IRI monthly median field of *M3000F2* is then corrected through Eq. (3):

$$IRI\_M3000F2_{\mathrm{STF,s,m,d,hh}} = IRI\_M3000F2_{\mathrm{MED\_PRED,s,m,hh}} + \Delta M\_BD_{\mathrm{STF,s,m,d,hh}}. \quad (5)$$

Given that in Eq. (5) the s index ranges between 1 and 12, Eq. (5) represents 12 short-term forecasting empirical local models able to provide short-term forecasts of *M3000F2* in diverse geomagnetic conditions because the predictions provided by Eq. (5) are connected with the short-term forecasts of *fo*F2. These models all together can be regarded as a single short-term forecasting empirical regional model to which henceforward we refer as *IRI_RM_M3000F2_BD*.

3 Description of the testing procedure comparisons and results

With a procedure analogous to that followed in Pietrella (2012), many epochs were selected for each ionospheric observatory over the years reported in column B of Table 1, and then grouped together. For these epochs the predictions of *M3000F2* calculated at each ionospheric observatory using the models represented by Eq. (2), Eq. (4), the IRI model, and Eq. (5) were binned in terms of three different ranges of geomagnetic activity: moderate ($7 < \mathrm{ap}(\tau = 0.8/0.9) \leq 20$), disturbed ($20 < \mathrm{ap}(\tau = 0.8/0.9) \leq 32$), and very disturbed ($\mathrm{ap}(\tau = 0.8/0.9) > 32$), where $\tau = 0.8$ is selected for the HLS, and $\tau = 0.9$ is preferred for the MLS and MHLS (the reason for which two different values of τ are used can be found in the paper of Pietrella, 2012). Subsequently, these data sets were binned by single month, and the performances of the forecasting procedures, Eq. (2), Eq. (4), the IRI model, and Eq. (5), were calculated and compared for each local station and for all the months in terms of global root mean square deviation (g.r.m.s.) error under moderate, disturbed and very disturbed geomagnetic conditions. An example of a flowchart describing the procedure followed to select the forecasting models providing the best performance in Tortosa for moderate geomagnetic conditions is shown in Fig. 2.

Figure 3 shows evidence of some ionospheric observatories and the related models providing the best performance for some months under moderate geomagnetic conditions.

Starting from tables such as that shown in Fig. 3, the sites for which each of the four forecasting models provides the best performance have been tabulated for each month under moderate (m), disturbed (d), and very disturbed (vd) geomagnetic activity to better realize how these models could be used for an operative approach (see Tables 2–5).

Since, as mentioned above, the set of forecasting local models can be regarded as a single forecasting empirical regional model, based on Tables 2–5, the percentages of the best performances given by the regional models *RM_M3000F2*, *RM_M3000F2_BD*, *IRI_RM_M3000F2*, and *IRI_RM_M3000F2_BD* have been also calculated for the three latitude intervals ($40^\circ\,\mathrm{N} \leq \lambda \leq 50^\circ\,\mathrm{N}$), ($50^\circ\,\mathrm{N} < \lambda \leq$

Table 2. The sites where the best performance is provided by the prediction model (2) are indicated with the full circle and shown for each month under moderate (m), disturbed (d), and very disturbed (vd) geomagnetic conditions. In these sites the different local models can be considered simultaneously operative for forecasting *M3000F2* over Europe. The columns labelled with MLS, MHLS, and HLS show the number of sites operating simultaneously located at middle ($40° \text{ N} \leq \lambda \leq 50° \text{ N}$), middle-high ($50° \text{ N} < \lambda \leq 60° \text{ N}$), and high latitudes ($60° \text{ N} < \lambda \leq 70° \text{ N}$) respectively.
The empty cells indicate cases that were discarded because the performance was worse than that of the others models. The values in the last column (T) indicate the total number of sites operating at the same time. The symbol $ indicates the cases in which the number of sites ($N < 4$) operating simultaneously is not considered satisfactory to cover the area under investigation. The term *nda* indicates the cases for which it was not possible to evaluate the performance of the prediction model (2) with respect to the other models because no data were available to calculate the g.r.m.s. error.

(a) Month	Tor MLS	Rom MLS	Poi MLS	Lan MLS	Dou MHLS	Slo MHLS	Jul MHLS	Kal MHLS	Upp MHLS	Lyc HLS	Sod HLS	Kir HLS	MLS	MHLS	HLS	T
Jan (m)	•	•	•		•		•	•	•				3	4	0	7
Feb (m)	•		•	•	•		•	•					3	3	0	6
Mar (m)								•					0	1	0	1 $
Apr (m)	•		•	•	•		•	•			•		3	3	1	7
May(m)	•		•	•	•	•	•	•		•	•		3	4	2	9
Jun (m)			•	•	•	•	•	•		•	•		2	4	2	8
Jul (m)			•	•	•		•	•			•		2	3	1	6
Aug (m)	•	•	•		•		•	•		•	•		3	3	2	8
Sep (m)	•		•	•	•		•	•		•	•		3	3	2	8
Oct (m)	•		•	•	•	•	•	•			•		3	4	1	8
Nov (m)	•		•	•	•	•	•						3	3	0	6
Dec (m)	•	•	•	•	•		•	•					4	3	0	7

(b) Month	Tor MLS	Rom MLS	Poi MLS	Lan MLS	Dou MHLS	Slo MHLS	Jul MHLS	Kal MHLS	Upp MHLS	Lyc HLS	Sod HLS	Kir HLS	MLS	MHLS	HLS	T
Jan (d)													0	0	0	0 $
Feb (d)								•					0	1	0	1 $
Mar (d)	•												1	0	0	1 $
Apr (d)	•		•	•			•	•					3	2	0	5
May (d)	•		•	•									3	0	0	3 $
Jun (d)							•						0	1	0	1 $
Jul (d)	•		•					•					2	1	0	3 $
Aug (d)													0	0	0	0 $
Sep (d)	•		•				•						2	1	0	3 $
Oct (d)				•									1	0	0	1 $
Nov (d)	•												1	0	0	1 $
Dec (d)		*nda*											0	0	0	0 $

(c) Month	Tor MLS	Rom MLS	Poi MLS	Lan MLS	Dou MHLS	Slo MHLS	Jul MHLS	Kal MHLS	Upp MHLS	Lyc HLS	Sod HLS	Kir HLS	MLS	MHLS	HLS	T
Jan (vd)		*nda*									*nda*		0	0	0	0 $
Feb(vd)		*nda*											0	0	0	0 $
Mar(vd)													0	0	0	0 $
Apr(vd)	•	*nda*	•	•				•					3	1	0	4
May(vd)	•			•				•			*nda*		2	1	0	3 $
Jun (vd)		*nda*									*nda*		0	0	0	0 $
Jul (vd)		*nda*			•						*nda*		0	1	0	1 $
Aug(vd)											*nda*		0	0	0	0 $
Sep(vd)	•			•									2	0	0	2 $
Oct(vd)		*nda*									•		0	0	1	1 $
Nov(vd)													0	0	0	0 $
Dec(vd)		*nda*											0	0	0	0 $

60° N), and ($60° \text{ N} < \lambda \leq 70° \text{ N}$). The results thus obtained are presented in the form of histograms in Fig. 4.

By adopting the criterion according to which a number $N \geq 4$ of operating stations is considered sufficient to adequately cover the area under investigation providing simultaneous predictions of *M3000F2*, it emerges that there are several cases where it is never possible to use operatively the models, the number of sites being $N < 4$ (see cases labelled with $). Therefore, from a careful inspection of Tables 2–5, we find that during moderate geomagnetic

Table 3. Same as Table 2 but for the sites where the best performance is provided by the prediction model (4), indicated with the triangle. The term *nda* indicates the cases for which it was not possible to evaluate the performance of the prediction model (4) with respect to the other models because no data were available to calculate the g.r.m.s. error.

(a) Month	Tor MLS	Rom MLS	Poi MLS	Lan MLS	Dou MHLS	Slo MHLS	Jul MHLS	Kal MHLS	Upp MHLS	Lyc HLS	Sod HLS	Kir HLS	MLS	MHLS	HLS	T
Jan(m)				▲		▲					▲		1	1	1	3 $
Feb(m)		▲	▲								▲		2	0	1	3 $
Mar(m)	▲	▲	▲		▲		▲						3	2	0	5
Apr(m)		▲											1	0	0	1 $
May(m)												▲	0	0	1	1 $
Jun (m)												▲	0	0	1	1 $
Jul (m)												▲	0	0	1	1 $
Aug(m)				▲					▲				1	1	0	2 $
Sep (m)	▲								▲			▲	1	1	1	3 $
Oct (m)		▲										▲	1	0	1	2 $
Nov(m)		▲										▲	1	0	1	2 $
Dec(m)						▲							0	1	0	1 $

(b) Month	Tor MLS	Rom MLS	Poi MLS	Lan MLS	Dou MHLS	Slo MHLS	Jul MHLS	Kal MHLS	Upp MHLS	Lyc HLS	Sod HLS	Kir HLS	MLS	MHLS	HLS	T
Jan (d)	▲		▲	▲			▲			▲			3	1	1	5
Feb (d)		▲	▲	▲		▲	▲						3	2	0	5
Mar (d)		▲	▲	▲			▲			▲			3	1	1	5
Apr (d)					▲								0	1	0	1 $
May (d)		▲			▲		▲			▲			1	2	1	4
Jun (d)			▲	▲	▲					▲	▲	▲	2	1	3	6
Jul (d)				▲			▲						1	1	0	2 $
Aug (d)			▲	▲			▲			▲			2	1	1	4
Sep (d)			▲		▲	▲		▲		▲			1	3	1	5
Oct (d)	▲		▲	▲	▲	▲	▲	▲		▲			3	4	1	8
Nov (d)		▲	▲	▲	▲	▲	▲			▲	▲		3	3	2	8
Dec (d)		*nda*	▲	▲	▲	▲	▲		▲	▲		▲	2	4	2	8

(c) Month	Tor MLS	Rom MLS	Poi MLS	Lan MLS	Dou MHLS	Slo MHLS	Jul MHLS	Kal MHLS	Upp MHLS	Lyc HLS	Sod HLS	Kir HLS	MLS	MHLS	HLS	T
Jan (vd)	▲	*nda*	▲						▲		*nda*		2	1	0	3 $
Feb (vd)		*nda*	▲	▲			▲						2	1	0	3 $
Mar (vd)		▲	▲	▲			▲						3	1	0	4
Apr (vd)		*nda*			▲	▲	▲			▲	▲		0	3	2	5
May (vd)			▲		▲	▲	▲			▲	*nda*		1	3	1	5
Jun (vd)		*nda*	▲	▲			▲	▲		▲	*nda*		2	2	1	5
Jul (vd)		*nda*	▲	▲			▲				*nda*		2	1	0	3 $
Aug(vd)			▲				▲				*nda*		1	1	0	2 $
Sep(vd)			▲				▲						1	1	0	2 $
Oct(vd)		*nda*	▲	▲			▲	▲		▲			2	2	1	5
Nov (vd)			▲	▲	▲		▲	▲		▲	▲		2	3	2	7
Dec (vd)	▲	*nda*	▲	▲						▲		▲	3	0	2	5

conditions *RM_M3000F2* is the model more suitable in providing forecasts of *M3000F2* because it ensures a very good coverage of the area under study with many sites operating at the same time (see Table 2a); the same cannot be said for *RM_M3000F2_BD*, *IRI_RM_M3000F2*, and *IRI_RM_M3000F2_BD*, which offer a very small number of sites simultaneously operative (see Tables 3a, 4a, and 5a). With regard to disturbed geomagnetic conditions, it is evident from Tables 2b and 4b that *RM_M3000F2* and *IRI_RM_M3000F2* are not appropriate for the operative use, because a more adequate coverage is provided by *RM_M3000F2_BD* (see Table 3b) although in some cases also *IRI_RM_M3000F2_BD* could be used (see Table 5b). As regards very disturbed geomagnetic conditions, also in this case *RM_M3000F2* and *IRI_RM_M3000F2* provide an absolutely inadequate coverage for the operative use (see Tables 2c and 4c), while *IRI_RM_M3000F2_BD* seems to be more appropriate for the operative use, assuring almost always a good coverage of the area under study (see Table 5c), even if in some cases also *RM_M3000F2_BD* could be used (see Table 3c).

Table 4. Same as Table 2 but for the sites where the best performance is provided by the IRI model, indicated with the empty circle. The term *nda* indicates the cases for which it was not possible to evaluate the performance of the IRI model with respect to the other models because no data were available to calculate the g.r.m.s. error.

(a) Month	Tor MLS	Rom MLS	Poi MLS	Lan MLS	Dou MHLS	Slo MHLS	Jul MHLS	Kal MHLS	Upp MHLS	Lyc HLS	Sod HLS	Kir HLS	MLS	MHLS	HLS	T
Jan (m)										○		○	0	0	2	2 $
Feb(m)									○	○		○	0	1	2	3 $
Mar (m)	○									○	○		1	0	2	1 $
Apr (m)						○							0	1	0	1 $
May (m)	○	○											2	0	0	2 $
Jun (m)	○	○											2	0	0	2 $
Jul (m)		○			○	○		○					1	3	0	4
Aug(m)					○	○							0	2	0	2 $
Sep (m)						○							0	1	0	1 $
Oct (m)									○	○			0	1	1	2 $
Nov (m)								○		○	○		0	1	2	3 $
Dec (m)									○		○		0	1	1	2 $

(b) Month	Tor MLS	Rom MLS	Poi MLS	Lan MLS	Dou MHLS	Slo MHLS	Jul MHLS	Kal MHLS	Upp MHLS	Lyc HLS	Sod HLS	Kir HLS	MLS	MHLS	HLS	T
Jan(d)		○			○			○					1	2	0	3 $
Feb (d)	○				○								1	1	0	2 $
Mar (d)					○			○			○		0	2	1	3 $
Apr (d)		○				○					○		1	1	1	3 $
May (d)								○			○		0	1	1	2 $
Jun (d)	○	○						○					2	1	0	3 $
Jul (d)		○									○		1	0	1	2 $
Aug (d)					○			○					0	2	0	2 $
Sep (d)		○						○					1	1	0	2 $
Oct (d)								○					0	1	0	1 $
Nov (d)	○							○					1	1	0	2 $
Dec (d)	○	*nda*						○					1	1	0	2 $

(c) Month	Tor MLS	Rom MLS	Poi MLS	Lan MLS	Dou MHLS	Slo MHLS	Jul MHLS	Kal MHLS	Upp MHLS	Lyc HLS	Sod HLS	Kir HLS	MLS	MHLS	HLS	T
Jan (vd)		*nda*									*nda*		0	0	0	0 $
Feb (vd)		*nda*											0	0	0	0 $
Mar (vd)								○					0	1	0	1 $
Apr (vd)		*nda*											0	0	0	0 $
May (vd)		○									*nda*		0	0	0	0 $
Jun (vd)		*nda*			○						*nda*		0	1	0	1 $
Jul (vd)	○	*nda*						○	○		*nda*		1	2	0	3 $
Aug (vd)	○	○			○						*nda*		2	1	0	3 $
Sep (vd)		○						○					1	1	0	2 $
Oct (vd)		*nda*											0	0	0	0 $
Nov (vd)	○												1	0	0	1 $
Dec (vd)		*nda*											0	0	0	0 $

Ultimately, on the basis of the results presented in Tables 2–5, it emerges that the more appropriate choice of the models to be considered for obtaining *M3000F2* predictions over the European area is (1) *RM_M3000F2* for moderate geomagnetic conditions (Table 2a); (2) *RM_M3000F2_BD* for disturbed geomagnetic conditions (Table 3b); and (3) *IRI_RM_M3000F2_BD* for very disturbed geomagnetic conditions (Table 5c).

Nevertheless, the observation of Tables 2a, 3b, and 5c shows also that such models are subject to the following two limitations: (a) the lack of MLS and HLS means that the model cannot provide a coverage of the area in the latitude ranges $40° \text{ N} \leq \lambda \leq 50° \text{ N}$ and $60° \text{ N} < \lambda \leq 70° \text{ N}$ respectively, and when this occurs the models provide *M3000F2* predictions in a more restricted area; (b) a totally inadequate coverage of the area emerges for some months, and in these cases it is not possible to provide *M3000F2* forecasts over the region under study.

Based on these considerations, Table 6 was built to clarify which models should be used and to better show evidence of their limits.

Table 5. Same as Table 2 but for the sites where the best performance is provided by the prediction model (5), indicated with the square. The term *nda* indicates the cases for which it was not possible to evaluate the performance of the prediction model (5) with respect to the other models because no data were available to calculate the g.r.m.s. error.

(a) Month	Tor MLS	Rom MLS	Poi MLS	Lan MLS	Dou MHLS	Slo MHLS	Jul MHLS	Kal MHLS	Upp MHLS	Lyc HLS	Sod HLS	Kir HLS	MLS	MHLS	HLS	T
Jan (m)													0	0	0	0 $
Feb (m)						■							0	1	0	1 $
Mar (m)				■		■			■			■	1	2	1	4
Apr (m)									■	■		■	0	1	2	3 $
May (m)									■				0	1	0	1 $
Jun (m)									■				0	1	0	1 $
Jul (m)		■							■	■			1	1	1	3 $
Aug (m)												■	0	0	1	1 $
Sep (m)													0	0	0	0 $
Oct (m)													0	0	0	0 $
Nov (m)									■				0	1	0	1 $
Dec (m)										■		■	0	0	2	2 $

(b) Month	Tor MLS	Rom MLS	Poi MLS	Lan MLS	Dou MHLS	Slo MHLS	Jul MHLS	Kal MHLS	Upp MHLS	Lyc HLS	Sod HLS	Kir HLS	MLS	MHLS	HLS	T
Jan (d)						■			■	■	■	■	0	2	3	5
Feb (d)									■	■	■	■	0	1	3	4
Mar (d)						■			■			■	0	2	1	3 $
Apr (d)									■	■		■	0	1	2	3 $
May (d)						■			■	■		■	0	2	2	4
Jun (d)						■			■				0	2	0	2 $
Jul (d)					■	■			■	■		■	0	3	2	5
Aug (d)	■	■				■			■		■	■	2	2	2	7
Sep (d)									■		■	■	0	1	2	3 $
Oct (d)		■							■		■	■	1	1	2	4
Nov (d)									■			■	0	1	1	2 $
Dec (d)		*nda*									■		0	0	1	1 $

(c) Month	Tor MLS	Rom MLS	Poi MLS	Lan MLS	Dou MHLS	Slo MHLS	Jul MHLS	Kal MHLS	Upp MHLS	Lyc HLS	Sod HLS	Kir HLS	MLS	MHLS	HLS	T
Jan (vd)		*nda*		■	■	■	■	■		■	*nda*	■	1	4	2	7
Feb (vd)	■	*nda*			■	■		■	■	■	■	■	1	4	3	8
Mar (vd)	■				■	■			■	■	■	■	1	3	3	7
Apr (vd)		*nda*			■				■			■	0	2	1	3 $
May (vd)									■		*nda*	■	0	1	1	2 $
Jun (vd)	■	*nda*				■			■		*nda*	■	1	2	1	4
Jul (vd)		*nda*				■				■	*nda*	■	0	1	2	3 $
Aug (vd)				■	■	■		■	■	■	*nda*	■	1	4	2	7
Sep (vd)						■			■	■	■	■	0	2	3	5
Oct (vd)	■	*nda*			■	■			■			■	1	3	1	5
Nov (vd)	■	■				■			■			■	2	2	1	5
Dec (vd)		*nda*			■	■	■	■	■		■		0	5	1	6

The limitations shown in bold in Table 6 and described at points (a) and (b) inherent to a given model could be removed or reduced using appropriately the other models. Under moderate geomagnetic conditions, *RM_M3000F2_BD* could be applied to provide *M3000F2* forecasts for the month of March, even if in a more restricted area because the HLS are missing.

Analogously, under disturbed geomagnetic conditions, *RM_M3000F2* and *IRI_RM_M3000F2_BD* could be used to calculate the values predicted of *M3000F2* for the months of April and July respectively; also in this case the coverage of the region under consideration will be limited by the lack of HLS (in April) and MLS (in July).

Similarly, under very disturbed geomagnetic conditions, *RM_M3000F2_BD* could replace *IRI_RM_M3000F2_BD* for providing *M3000F2* predictions for the months of April (in a more restricted region because the MLS are missing) and May. Therefore, in the light of these latest considerations, a possible table for an operative use was built (see Table 7).

Figure 5 shows the comparison between the map based on *M3000F2* measurements (Fig. 5a) and the map based on the

Table 6. Use of *RM_M3000F2*, *RM_M3000F2_BD*, and *IRI_RM_M3000F2_BD* under **(a)** moderate, **(b)** disturbed, and **(c)** very disturbed geomagnetic conditions respectively. The months for which *M3000F2* predictions are provided over a more restricted area because of the lack of MLS or HLS, and the months where the model is not able to assure a coverage of the area under consideration because of the lack of an adequate number of sites operating at the same time, are marked in bold and underlined bold respectively.

(a) Month	Tor MLS	Rom MLS	Poi MLS	Lan MLS	Dou MHLS	Slo MHLS	Jul MHLS	Kal MHLS	Upp MHLS	Lyc HLS	Sod HLS	Kir HLS	MLS	MHLS	HLS	T
Jan (m)	•	•	•		•		•	•	•				3	4	**0**	7
Feb (m)	•		•	•	•		•	•					3	3	**0**	6
Mar (m)								•					0	1	0	**1 $**
Apr (m)	•		•	•	•		•	•			•		3	3	1	7
May (m)	•		•	•	•	•	•	•		•	•		3	4	2	9
Jun (m)			•	•	•	•	•	•		•	•		2	4	2	8
Jul (m)			•	•	•		•	•			•		2	3	1	6
Aug (m)	•	•	•		•		•	•		•	•		3	3	2	8
Sep (m)	•		•	•	•		•	•		•	•		3	3	2	8
Oct (m)	•		•	•	•	•	•	•			•		3	4	1	8
Nov (m)	•		•	•	•	•	•						3	3	**0**	6
Dec (m)	•	•	•	•	•		•	•					4	3	**0**	7

(b) Month	Tor MLS	Rom MLS	Poi MLS	Lan MLS	Dou MHLS	Slo MHLS	Jul MHLS	Kal MHLS	Upp MHLS	Lyc HLS	Sod HLS	Kir HLS	MLS	MHLS	HLS	T
Jan (d)	▲		▲	▲			▲			▲			3	1	1	5
Feb (d)		▲	▲	▲		▲	▲						3	2	**0**	5
Mar (d)		▲	▲	▲			▲			▲			3	1	1	5
Apr (d)					▲								0	1	0	**1 $**
May (d)		▲			▲		▲			▲			1	2	1	4
Jun (d)			▲	▲	▲					▲	▲	▲	2	1	3	6
Jul (d)				▲			▲						1	1	0	**2 $**
Aug (d)			▲	▲			▲			▲			2	1	1	4
Sep (d)			▲		▲	▲		▲		▲			1	3	1	5
Oct (d)	▲		▲	▲	▲	▲	▲	▲		▲			3	4	1	8
Nov (d)		▲	▲	▲	▲	▲	▲			▲	▲		3	3	2	8
Dec (d)			▲	▲	▲	▲	▲		▲	▲		▲	2	4	2	8

(c) Month	Tor MLS	Rom MLS	Poi MLS	Lan MLS	Dou MHLS	Slo MHLS	Jul MHLS	Kal MHLS	Upp MHLS	Lyc HLS	Sod HLS	Kir HLS	MLS	MHLS	HLS	T
Jan (vd)				■	■	■	■	■		■		■	1	4	2	7
Feb (vd)	■				■	■		■	■	■	■	■	1	4	3	8
Mar (vd)	■				■	■			■	■	■	■	1	3	3	7
Apr (vd)					■				■			■	0	2	1	**3 $**
May (vd)									■			■	0	1	1	**2 $**
Jun (vd)	■					■			■			■	1	2	1	4
Jul (vd)						■				■		■	0	1	2	**3 $**
Aug (vd)				■	■	■		■	■	■		■	1	4	2	7
Sep (vd)						■			■	■	■	■	**0**	2	3	5
Oct (vd)	■				■	■			■			■	1	3	1	5
Nov (vd)	■	■				■			■			■	2	2	1	5
Dec (vd)					■	■	■	■	■		■		**0**	5	1	6

long-term predictions of *M3000F2* (Fig. 5b) obtained with the 9 forecasting local models simultaneously operative for the month of May (see Table 7a). The epoch under consideration, characterized by moderate geomagnetic activity, is 18 May 1991 at 01:00 UT.

Figures 6 and 7 show comparisons between the maps based on *M3000F2* measurements (Figs. 6a–7a) and the maps based on the short-term forecasting of *M3000F2* under disturbed/very disturbed geomagnetic activity (Figs. 6b–7b) obtained with the *RM_M3000F2_BD* /*IRI_RM_M3000F2_BD* regional models respectively.

To get the short-term forecasting map of *M3000F2* during disturbed geomagnetic conditions (Fig. 6b), *RM_M3000F2_BD* has taken into account the 8 forecasting local models simultaneously operative for the month of November shown in Table 7b. The epoch under consideration is 16 November 1991 at 01:00 UT.

The short-term forecasting map of *M3000F2* under very disturbed geomagnetic conditions (Fig. 7b) was derived from

Table 7. Same as Table 6, but with some improvements for a possible operative use.

(a) Month	Tor MLS	Rom MLS	Poi MLS	Lan MLS	Dou MHLS	Slo MHLS	Jul MHLS	Kal MHLS	Upp MHLS	Lyc HLS	Sod HLS	Kir HLS	MLS	MHLS	HLS	T
Jan (m)	•	•	•		•		•	•	•				3	4	**0**	7
Feb (m)	•		•	•	•		•	•					3	3	**0**	6
Mar (m)	▲	▲	▲		▲		▲						3	2	**0**	5
Apr (m)	•		•	•	•		•	•			•		3	3	1	7
May (m)	•		•	•	•	•	•	•		•	•		3	4	2	9
Jun (m)			•	•	•	•	•	•		•	•		2	4	2	8
Jul (m)			•	•	•		•	•			•		2	3	1	6
Aug (m)	•	•	•		•		•	•		•	•		3	3	2	8
Sep (m)	•		•	•	•		•	•		•	•		3	3	2	8
Oct (m)	•		•	•	•	•	•	•			•		3	4	1	8
Nov (m)	•		•	•	•	•	•						3	3	**0**	6
Dec (m)	•	•	•	•	•		•	•					4	3	**0**	7

(b) Month	Tor MLS	Rom MLS	Poi MLS	Lan MLS	Dou MHLS	Slo MHLS	Jul MHLS	Kal MHLS	Upp MHLS	Lyc HLS	Sod HLS	Kir HLS	MLS	MHLS	HLS	T
Jan (d)	▲		▲	▲			▲			▲			3	1	1	5
Feb (d)		▲	▲	▲		▲	▲						3	2	**0**	5
Mar (d)		▲	▲	▲			▲			▲			3	1	1	5
Apr (d)	•		•	•			•	•					3	2	**0**	5
May (d)		▲			▲		▲			▲			1	2	1	4
Jun (d)			▲	▲	▲					▲	▲	▲	2	1	3	6
Jul (d)					■	■			■	■		■	**0**	3	2	5
Aug (d)			▲	▲			▲			▲			2	1	1	4
Sep (d)			▲		▲	▲		▲		▲			1	3	1	5
Oct (d)	▲		▲	▲	▲	▲	▲	▲		▲			3	4	1	8
Nov (d)		▲	▲	▲	▲	▲	▲			▲	▲		3	3	2	8
Dec (d)			▲	▲	▲	▲	▲		▲	▲		▲	2	4	2	8

(c) Month	Tor MLS	Rom MLS	Poi MLS	Lan MLS	Dou MHLS	Slo MHLS	Jul MHLS	Kal MHLS	Upp MHLS	Lyc HLS	Sod HLS	Kir HLS	MLS	MHLS	HLS	T
Jan (vd)				■	■	■	■	■		■		■	1	4	2	7
Feb (vd)	■				■	■		■	■	■	■	■	1	4	3	8
Mar (vd)	■				■	■			■	■	■	■	1	3	3	7
Apr (vd)					▲	▲	▲			▲	▲		**0**	3	2	5
May (vd)			▲		▲	▲	▲			▲			1	3	1	5
Jun (vd)	■					■			■			■	1	2	1	4
Jul (vd)						■				■		■	0	1	2	**3 $**
Aug (vd)				■	■	■		■	■	■		■	1	4	2	7
Sep (vd)						■			■	■	■	■	**0**	2	3	5
Oct (vd)	■				■	■			■			■	1	3	1	5
Nov (vd)	■	■				■			■			■	2	2	1	5
Dec (vd)					■	■	■	■	■		■		**0**	5	1	6

IRI_RM_M3000F2_BD using the 8 forecasting local models operating at the same time for the month of February indicated in Table 7c. The epoch under consideration is 4 February 1992 at 17:00 UT.

4 Discussion of the results and future developments

The very small number of sites providing the best predictions observed in Tables 2b–c/3a,5a/4a–c indicates that in these cases it is not possible to consider the forecasting local models as a single forecasting empirical regional model able to offer an adequate coverage of the area when disturbed and very disturbed/moderate/moderate, disturbed and very disturbed geomagnetic conditions occur.

Anyway from the observation of Tables 2–5 emerges that it is never possible to work with all the 12 stations simultaneously.

Nevertheless, the strong point of this method is that, even not including certain stations, it is almost always possible to find a number $N < 12$ of local models offering an adequate coverage of the European area.

Therefore by adopting the criterion according to which a number $N \geq 4$ of operating stations is considered sufficient to adequately cover the area under investigation providing simultaneous predictions of *M3000F2*, Tables 3a/5a show that,

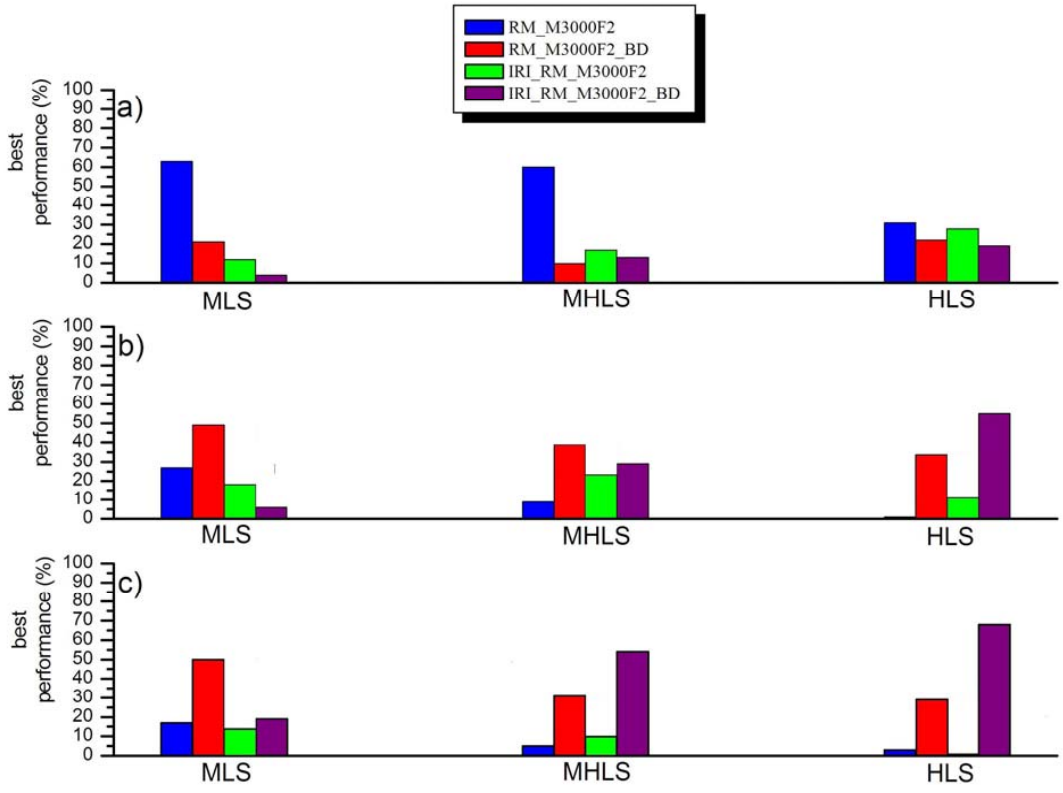

Fig. 4. The percentages of the best performances offered by *RM_M3000F2*, *RM_M3000F2_BD*, *IRI_RM_M3000F2*, and *IRI_RM_M3000F2_BD* deduced from Tables 2–5 are shown in blue, red, green, and purple respectively in the case of **(a)** moderate, **(b)** disturbed, and **(c)** very disturbed geomagnetic activity for MLS, MHLS, and HLS.

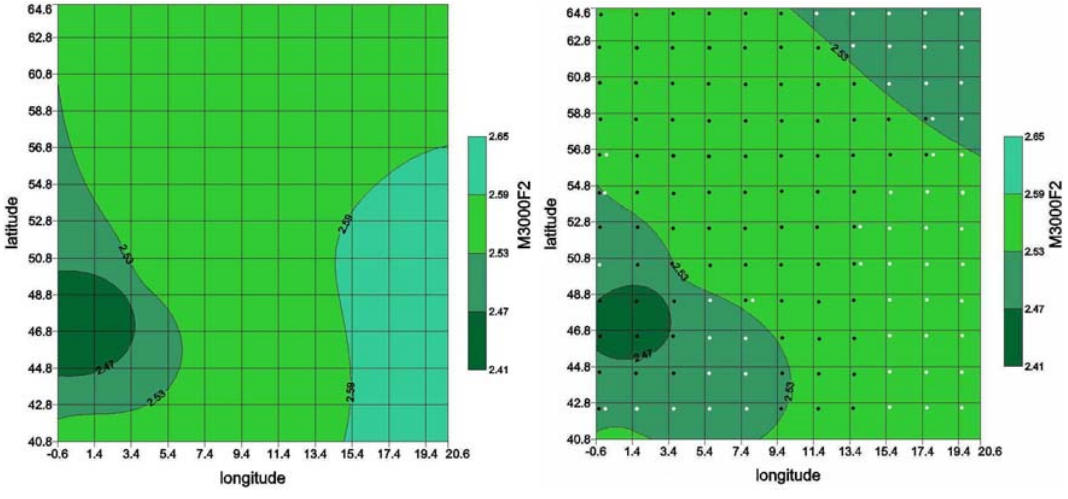

(a) (b)

Fig. 5. (a) Map obtained from *M3000F2* measurements and **(b)** long-term prediction map for *M3000F2* generated using the 9 forecasting local models simultaneously operative for the month of May (see Table 7a). The epoch under consideration, characterized by moderate geomagnetic activity ($ap(\tau = 0.8) = 17.9$; $ap(\tau = 0.9) = 18.1$), is 18 May 1991 at 01:00 UT. The white circles indicate the cells where the predictions of *M3000F2* are less satisfactory. The black circles indicate the cells where the predictions of *M3000F2* quite faithfully match the *M3000F2* measurements. The cells labelled with both the circles indicate that the performance can be considered satisfactory only in part of the cell.

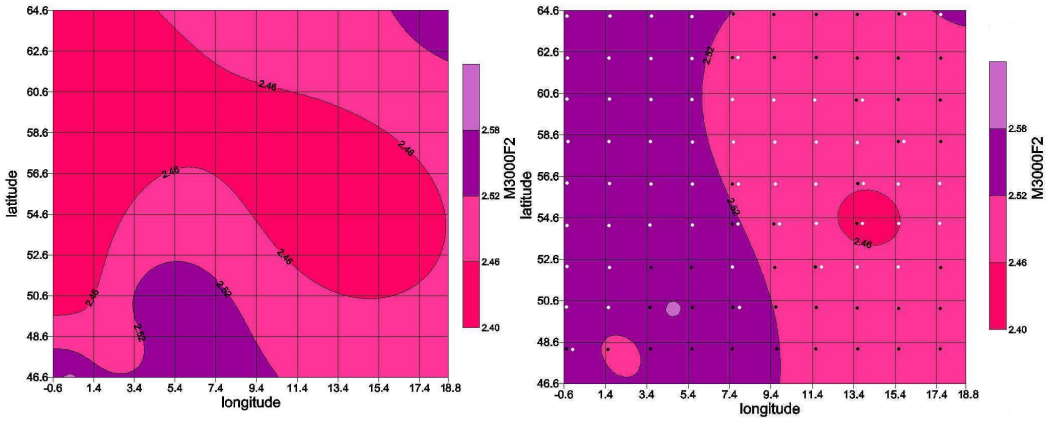

Fig. 6. Same as Fig. 5 but for a short-term forecasting of *M3000F2* generated one hour in advance on 16 November 1991 at 01:00 UT under disturbed geomagnetic activity (ap($\tau = 0.8$) = 24.8; ap($\tau = 0.9$) = 20.5) using the 8 forecasting local models simultaneously operative for the month of November (see Table 7b).

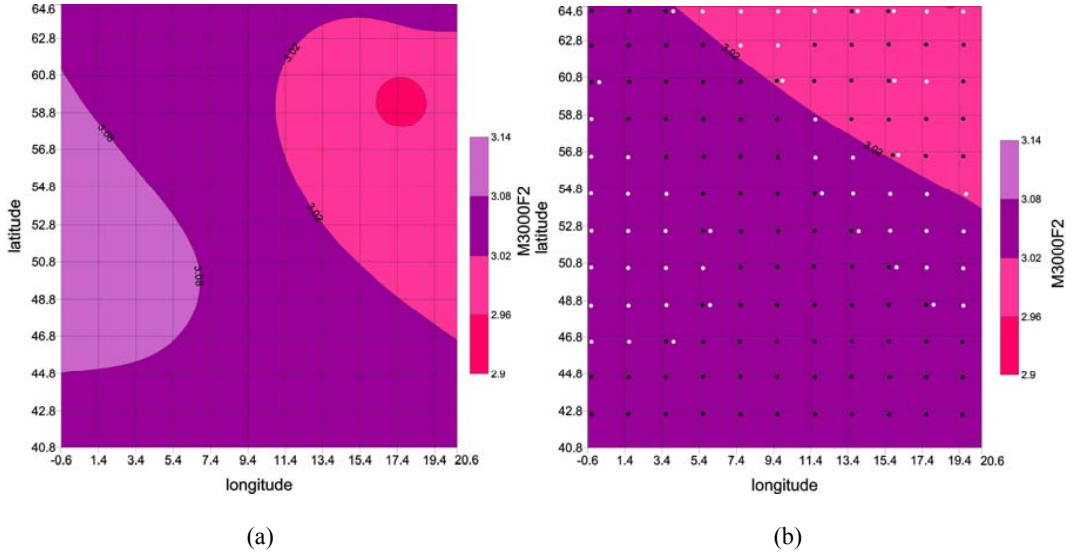

Fig. 7. Same as Fig. 5 but for a short-term forecasting of *M3000F2* generated two hours in advance on 4 February 1992 at 17:00 UT under very disturbed geomagnetic activity (ap($\tau = 0.8$) = 35.4; ap($\tau = 0.9$) = 41.2) using the 8 forecasting local models simultaneously operative for the month of February (see Table 7c).

except for the month of March where 5/4 stations are simultaneously operative, in all the other cases (marked with \$) it is never possible to use operatively the prediction models represented by Eqs. (4) and (5). This occurs because the Bradley–Dudeney algorithm is not effective in improving the monthly median field generated by Eq. (2) and the IRI model during moderately disturbed conditions.

This implies that moderate geomagnetic conditions cannot be considered so different from quiet geomagnetic conditions, and hence the short-term forecasting of *M3000F2* under moderate geomagnetic activity can be practically represented by the long-term predictions of *M3000F2*. Therefore under moderate geomagnetic conditions it is sufficient to use the forecasting models operating at the same time in the sites shown in Table 2a in order to get for all the months (except for March) the best short-term forecasts of *M3000F2*.

However, under disturbed geomagnetic activity, the Bradley–Dudeney correction factor is able to improve significantly the performance of the local models whose predictions are provided by Eq. (2). In fact for disturbed geomagnetic conditions, excluding the two cases relative to April and July, in the remaining ten cases there are always a sufficient number of sites that can operate simultaneously providing an adequate coverage of the European area (see Table 3b). With regard to very disturbed geomagnetic activity, again the Bradley–Dudeney formula improves noticeably the IRI

performance given that, excluding the three cases relative to April, May, and July, in all the remaining cases the forecasting models operating at the same time in the sites shown in Table 5c can work all together providing simultaneous predictions of *M3000F2* in the considered area.

Even though IRI local models provide the worst performance, as can be deduced from the observations of Table 4 and Fig. 4, nevertheless it is noteworthy that, under very disturbed geomagnetic conditions, the Bradley–Dudeney formula adopted to correct IRI model predictions improves considerably the performance of IRI local models especially for the MHLS and HLS (see Table 5 and Fig. 4).

As already explained in Sect. 3, the restrictions highlighted in Table 6 have been mitigated and a new table which could be adopted for a possible operative use was obtained (see Table 7). This means that the forecasting local models represented by Eqs. (2), (4), and (5) could be used as a single forecasting empirical regional model *RM_M3000F2*/*RM_M3000F2_BD*/*IRI_RM_M3000F2_BD* for generating forecasting maps of *M3000F2* up to 3 h in advance, under moderate/disturbed/very disturbed geomagnetic conditions over the European area on the basis of *M3000F2* predictions produced by those local stations that can be considered as simultaneously operative (see Table 7).

Just to clarify better the question, the *RM_M3000F2* regional model utilized to generate at the same time *M3000F2* forecasts in May for moderate geomagnetic activity is constituted by $N = 9$ stations leaving out the workstations of Rome, Uppsala, and Kiruna (see Table 7a); the *RM_M3000F2_BD* regional model employed to produce simultaneous predictions of *M3000F2* in November for disturbed geomagnetic activity is formed by $N = 8$ stations excluding the stations of Tortosa, Kaliningrad, Uppsala, and Kiruna (see Table 7b); and the *IRI_RM_M3000F2_BD* regional model used to get *M3000F2* forecasts in February for very disturbed geomagnetic activity could work with $N = 8$ sites operating at the same time leaving inoperative the stations of Rome, Poitiers, Lannion, and Juliusruh (see Table 7c).

Table 7 shows 1 case for disturbed geomagnetic conditions (July) and 3 cases for very disturbed geomagnetic conditions (April, September, and December) for which it is not possible to rely on the MLS for the prediction of *M3000F2*. This implies that the remaining sites operating at the same time will provide forecasts of *M3000F2* over a more limited European area extending in latitude from 50°1′ N to 67°8′ N and in longitude from −0°6′ W to 26°6′ E. Analogously, in Table 7 are shown 5 cases for moderate geomagnetic activity (January, February, March, November, and December) and 2 cases for disturbed geomagnetic conditions (February and April) in which it is not possible to rely on the HLS for the prediction of *M3000F2*. Therefore in these cases the remaining sites operating simultaneously will provide forecasts of *M3000F2* over a more restricted European sector extending in latitude from 40°8′ N to 59°8′ N and in longitude from −0°6′ W to 20°6′ E.

A careful analysis of the performance of the various models shown in Fig. 4, leads to the following conclusions.

As regards the MLS of the European area under consideration (Tortosa, Rome, Poitiers, and Lannion), extending in latitude from 40°8′ N to 48°1′ N and in longitude from 0°3′ W to 12°5′ E, overall the following considerations can be done: in the case of moderate geomagnetic activity, the performance of *RM_M3000F2* is markedly better than *RM_M3000F2_BD*, *IRI_RM_M3000F2*, and *IRI_RM_M3000F2_BD* being the predictions better in 63, 21, 12, and 4 % of the cases analysed respectively. This means that the local models are much more reliable than IRI models and the correction by the Bradley–Dudeney formula does not contribute to improve the performance.

In the case of disturbed geomagnetic activity, *RM_M3000F2*, *IRI_RM_M3000F2*, and *IRI_RM_M3000F2_BD* do not provide good performance because their predictions were better only in 27, 18, and 6 % of the cases analysed respectively, but the Bradley–Dudeney formula applied to correct the predictions of the local models seems to be effective in improving the predictions given that the *RM_M3000F2_BD* performance is better in 49 % of cases.

In the case of very disturbed geomagnetic activity, *RM_M3000F2*, *IRI_RM_M3000F2*, and *IRI_RM_M3000F2_BD* provide a very modest performance, with their predictions being better in only 17, 14, and 19 % of the cases analysed respectively; conversely, the *RM_M3000F2* performance is improved with the Bradley–Dudeney correction given that *RM_M3000F2_BD* provides better predictions in 50 % of cases.

With regard to the MHLS of the European area under study (Dourbes, Slough, Juliusruh, Kaliningrad, and Uppsala), extending in latitude from 50°1′ N to 59°8′ N and in longitude from −0°6′ E to 20°6′ E, in general the following considerations can be drawn: in the case of moderate geomagnetic activity, *RM_M3000F2* performance is noticeably better than *RM_M3000F2_BD*, *IRI_RM_M3000F2*, and *IRI_RM_M3000F2_BD* because the predictions provided by *RM_M3000F2* were better in 60 % of cases, while the predictions obtained with *RM_M3000F2_BD*, *IRI_RM_M3000F2*, and *IRI_RM_M3000F2_BD* were better in only 10 %, 17 %, and 13 % of the cases analysed respectively. This means that the local models are much more reliable than IRI models and the correction by the Bradley–Dudeney formula does not contribute significantly to improve the performance.

In the case of disturbed geomagnetic activity, *RM_M3000F2* and *IRI_RM_M3000F2* do not provide good performance, their predictions were better only in 9 and 23 % of the cases analysed; the Bradley–Dudeney formula improves slightly the predictions because the *RM_M3000F2_BD* and *IRI_RM_M3000F2_BD*

performance is better in 39 % and 29 % of the cases analysed respectively.

In the case of very disturbed geomagnetic activity, *RM_M3000F2* and *IRI_RM_M3000F2* provide a very poor performance, with their predictions being better only in 5 and 10 % of the cases analysed respectively; contrarily, *RM_M3000F2_BD* and *IRI_RM_M3000F2_BD* performance improves considerably by means of the Bradley–Dudeney correction factor especially for *IRI_RM_M3000F2_BD*. The predictions provided by *RM_M3000F2_BD*/*IRI_RM_M3000F2_BD* were better in 31 %/54 % of the cases analysed.

Regarding the HLS of the European area under consideration (Lyckesele, Sodankyla, and Kiruna), extending in latitude from 64°6′ N to 67°8′ N and in longitude from 18°8′ E to 26°6′ E, the following general considerations can be done: in the case of moderate geomagnetic activity, even though the *RM_M3000F2* performance is superior with respect to *RM_M3000F2_BD*/*IRI_RM_M3000F2*/*IRI_RM_M3000F2 _BD*, it is not significantly better than in the previous cases, providing better predictions in 31 % of cases in comparison with 22 %/28 %/19 %. In the case of disturbed geomagnetic activity, *RM_M3000F2*/*IRI_RM_M3000F2* provide a very poor performance because their predictions were better in only 0 %/11 % of the cases analysed, but the predictions greatly improve by using the Bradley–Dudeney formula because *RM_M3000F2_BD*/*IRI_RM_M3000F2_BD* forecasts were better in 34 %/55 % of the cases analysed.

A very poor performance is also given by *RM_M3000F2* and *IRI_RM_M3000F2* in the case of very disturbed geomagnetic activity, because their predictions were better in only 3 % and 0 % of the cases analysed respectively; conversely, the Bradley–Dudeney correction factor used to correct *RM_M3000F2*/*IRI_RM_M3000F2* has proved very efficient to get better predictions given that the *RM_M3000F2_BD*/*IRI_RM_M3000F2_BD* performance increases noticeably, providing better predictions in 29 %/68 % of the cases analysed.

Figure 5 shows the comparison between the map based on *M3000F2* measurements (Fig. 5a) and the map based on the long-term predictions of *M3000F2* (Fig. 5b), obtained with the 9 forecasting local models simultaneously operative for the month of May (see Table 7a). It must be said that at the considered epoch (18 May 1991 at 01:00 UT), *M3000F2* measurement at Sodankyla is missing and it cannot be compared with the corresponding prediction. Since a comparison between measurement and prediction for each station is needed, to compare directly the map of the measurements with the map of the predictions, the prediction of *M3000F2* at Sodankyla was not considered; for this reason the maps in Fig. 5 are presented in a more limited area.

To get the short-term forecasting map of *M3000F2* during disturbed geomagnetic conditions (Fig. 6b), *RM_M3000F2_BD* has taken into account the 8 forecasting local models simultaneously operative for the month of November shown in Table 7b. It must be noted that at the considered epoch (16 November 1991 at 01:00 UT), *M3000F2* measurements at Rome and Sodankyla are not available and therefore they cannot be compared with the corresponding predictions. Because of this the predictions of *M3000F2* at Rome and Sodankyla were not considered, and for this reason the maps in Fig. 6 are presented in a more restricted area.

Under very disturbed geomagnetic conditions, the short-term forecasting map of *M3000F2* was obtained from the *M3000F2* predictions derived from the 8 forecasting local models operating at the same time for the month of February and shown in Table 7c. *M3000F2* predictions at Sodankyla and Kiruna were not considered to build the map because the respective *M3000F2* measurements at the considered epoch (4 February 1992 at 17:00 UT) are missing; consequently also in this case the maps in Fig. 7 are represented in a narrower region.

The cells of these maps (see Figs. 5–7), depicted with a step in latitude and longitude of 2°, were scrupulously examined to evaluate the reliability of the models on the spatial regional scale.

Under moderate geomagnetic conditions (Fig. 5a–b), it emerged that there is a very large area extending in latitude from 40°8′ N to 64°6′ N and in longitude from −0°6′ W to 15°4′ E, where the *RM_M3000F2* performance can be considered very satisfactory because 83 % of this area shows that the differences between *M3000F2* measurements and *M3000F2* predictions differ by no more than 0.06. The performance of *RM_M3000F2* goes down in the sector extending in latitude from 40°8′ N to 64°6′ N and in longitude from 15°4′ E to 20°6′ E where the differences between *M3000F2* measurements and *M3000F2* predictions are no larger than 0.12. In terms of the three latitudinal ranges, *RM_M3000F2* performance can be considered good because the 53 %, 73 %, and 64 % of sectors located at middle, middle-high and high latitudes respectively show differences between *M3000F2* measurements and *M3000F2* predictions no greater than 0.06.

From the comparison between the map obtained with the *M3000F2* measurements and the short-term forecasting map generated by *RM_M3000F2_BD* under disturbed geomagnetic conditions (Fig. 6a–6b), two sectors, one extending in latitude from 46°6′ N to 52°6′ N and in longitude from −0°6′ W to 18°8′ E, and the other one extending in latitude from 58°6′ N to 64°6′ N and in longitude from 7°4′ E to 18°8′ E, show a very satisfactory performance of *RM_M3000F2_BD* because in 70 % of the area covered by these sectors the differences between the *M3000F2* measurements and *M3000F2* forecasts are no larger than 0.06.

The performance of *RM_M3000F2_BD* deteriorates slightly in the zone extending in latitude from 52°6′ N to 58°6′ N and in longitude from 7°4′ E to 18°8′ E where, except in some small areas, the differences between *M3000F2* measurements and *M3000F2* forecasts are no greater than

0.12. *RM_M3000F2_BD* performance worsens further in the sector extending in latitude from 52°6′ N to 64°6′ N and in longitude from −0°6′ W to 7°4′ E where 70 % of this area shows differences between *M3000F2* measurements and *M3000F2* predictions no bigger than 0.18. Reasoning in terms of the three different latitudinal sectors the following considerations can be done: the 85 % of the sector situated at middle latitudes shows a very satisfactory performance because *M3000F2* measurements and *M3000F2* forecasts differ by no more than 0.06; the performance is not very good in the area sited at middle-high latitudes where only 31 % of this area shows differences between measurements and predictions no greater than 0.06; an improvement of the performance can be observed at high latitudes because 42 % of this sector shows differences no larger than 0.06.

Under very disturbed geomagnetic conditions (Fig. 7a–b), in a relatively large area extending in latitude from 40°8′ N to 64°6′ N and in longitude from −0°6′ W to 5°4′ E, *IRI_RM_M3000F2_BD* performance is not very good because only 49 % of this area shows differences between *M3000F2* measurements and M*3000F2* predictions no larger than 0.06.

However, a very satisfactory performance is observed in the region extending in latitude from 40°8′ N to 64°6′ N and in longitude from 5°4′ E to 20°6′ E, because 70 % of this region shows variations between *M3000F2* measurements and *M3000F2* predictions no larger than 0.06. In terms of the three latitudinal ranges, a high performance is observed in the area situated at middle latitudes where the 75 % of this area shows differences between *M3000F2* measurements and *M3000F2* forecasts no greater than 0.06. The performance worsens, but it can be still considered good at middle-high and high latitudes because the 55 %, and 64 % of these sectors show differences between *M3000F2* measurements and *M3000F2* forecasts no greater than 0.06.

According to the criterion that has been adopted, in the special case of July under very disturbed geomagnetic conditions (see Table 7c), the number of stations operating at the same time is not considered sufficient to ensure an adequate coverage, and therefore in this unique case it is not possible to provide *M3000F2* forecasts for the European area.

As a rule, when A workstations are put aside, the *M3000F2* forecasts are calculated in the remaining $(N - A)$ workstations. Starting from the predictions of *M3000F2* generated at certain epochs by the $(N - A)$ local models, and conceiving the area considered in this study as a grid of equispaced points in latitude and longitude, it is possible using a suitable interpolation algorithm to compute the values of *M3000F2* also at the A workstations that were initially rejected as well as the values of *M3000F2* at each grid point. The elaboration of *M3000F2* data thus obtained permits the achievement of short-term forecasting maps of *M3000F2* at the epochs under consideration.

With regard to the three *M3000F2* forecasting maps considered in this study (Figs. 5–7), in some regions located at middle, middle-high, and high latitudes, the performance of *RM_M3000F2*, *RM_M3000F2_BD*, and *IRI_RM_M3000F2_BD* does not give fine results (see in Figs. 5b–7b the cells labelled with the white circle). This probably occurs because the prediction algorithm is composed by a monthly median model corrected with a factor that depends on the short-term forecasting of *foF2*, so that the prediction of *M3000* is inevitably affected by an error that is the sum of the errors committed by the monthly median model and short-term forecasting model of *fo*F2. Nevertheless, from the forecasting maps produced by *RM_M3000F2*, *RM_M3000F2_BD*, and *IRI_RM_M3000F2_BD* it is also possible to note wide zones situated at middle, middle-high, and high latitudes where the *RM_M3000F2*, *RM_M3000F2_BD*, and *IRI_RM_M3000F2_BD* predictions agree quite well with the *M3000F2* measurements (see in Figs. 5b–7b the cells labelled with the black circles). This is a satisfactory result because it is not easy to yield reliable predictions when not quiet geomagnetic conditions occur, particularly at high latitudes.

With regard to future developments, an operative use of Table 7 would allow the regional models *RM_M3000F2*, *RM_M3000F2_BD*, and *IRI_RM_M3000F2_BD* to generate short-term forecasting maps of *M3000F2* up to 3 h in advance over Europe on the basis of *M3000F2* predictions produced by those local stations that can be considered as simultaneously operative.

Moreover, in spite of some limitations described above, the short-term forecasting models of *M3000F2* developed in this work could be used together with the *IFERM_foF2* model providing short-term forecasts of *fo*F2 (Pietrella, 2012). The predictions of *M3000F2* and *fo*F2 thus obtained, given as input parameters to the IRI model, can provide a short-term forecasting of 3-D electron density mapping of the ionosphere over the European area following a technique similar to that recently utilized to achieve quasi-real-time maps of electron density over the Mediterranean region (Pezzopane et al., 2011).

The realization of short-term forecasting maps of *M3000F2* together with 3-D matrices of electron density up to three hours in advance over Europe is one of the aims to be achieved in the future. In addition, the values of *M3000F2* predicted with these models and the values of *fo*F2 predicted by *IFERM_foF2* could also be used to calculate short-term forecasts of the height of the maximum electron density of the F2 layer (*hm*F2) in all the operative sites. The achievement of short-term forecasting maps of *hm*F2 based on the predictions of *hm*F2 during moderate, disturbed and very disturbed geomagnetic conditions is another target to be achieved in the future.

Acknowledgements. The author is grateful to the anonymous referee for their suggestions that contributed to improving the paper. The author would like also to thank S. Spadoni for the help provided in downloading M3000F2 data from IRI model as well as for her assistance in producing the maps of M3000F2.

Topical Editor K. Hosokawa thanks L. Cander and one anonymous referee for their help in evaluating this paper.

References

Araujo-Pradere, E. A., Fuller-Rowell, T. J., and Codrescu, M. V.: STORM: an empirical storm-time ionospheric correction model 1. Model description, Radio Sci., 37, 1070, doi:10.1029/2001RS002467, 2002.

Bilitza, D.: International Reference Ionosphere 2000, Radio Sci., 36, 261–276, doi:10.1029/2000RS002432, 2001.

Bilitza, D.: Ionospheric models for radio propagation studies, in: The Review of Radio Science 1999–2002: Advances in 3G Mobile Communications,Cryptography and Computer Security, EMC for Integrated Circuits, Remote Sensing, Radio Astronomy and More, edited by: Stone, W. R., 625–680, IEEE Press, Piscataway, N. Y, 2002.

Bilitza, D. and Reinisch, B. W.: International Reference Ionosphere 2007: Improvements and new parameters, Adv. Space Res., 42, 599–609, doi:10.1016/j.asr.2007.07.048, 2008.

Bradley, P. A.: PRIME (Prediction and Retrospective Ionospheric Modelling over Europe), Cost Action 238, Final Report, Rutherford Appleton Laboratory, Chilton Didcot, UK, 1999.

Bradley, P. A. and Dudeney, J. R.: A simple model of the vertical distribution of the electron concentration in the ionosphere, J. Atmos. Terr. Phys, 35, 2131–2146, 1973.

Cander, L. R.: Toward forecasting and mapping ionospheric space weather under cost actions, Adv. Space Res., 31, 957–964, doi:10.1016/S0273-1177(02)00793-7, 2003.

Cander, L. R.: Ionospheric research and space weather services, J. Atmos. Sol. Terr. Phys., 70, 1870–1878, doi:10.1016/j.jastp.2008.05.010, 2008.

Cander, Lj. R., Milosavljevic, M. M., Stankovic, S. S., and Tomasevic, S.: Ionospheric forecasting technique by artificial neural network, Electronics Lett., 34, 1573–1574, 1998.

Cander, L. R., Milosavljevic, M. M., and Tomasevic, S.: Ionospheric forecasting technique by artificial neural network, Ann. Geophys., 46, 719–724, 2003.

Chen, C., Wu, Z. S., Zhao, Z. W., Sun, S. J., and Xi, D. L.: A short term *fo*F2 forecasting method based on neural network techniques, Chin. J. Radio Sci., 23, 708–712, 2008.

Comite Consultatif International des Radio Communications (CCIR): Atlas of ionospheric characteristics, Rep 340-6 Geneva, 1991.

De Franceschi, G., Perrone, L., and Pau, S.: The SWILM approach for regional long-term modelling of middle/high latitude ionosphere, Phys. Chem. Earth., 25, 343–346, 2000.

Francis, N. M., Brown, A. G., Cannon, P. S., and Broomhead, D. S.: Prediction of the hourly ionospheric parameter *fo*F2 a novel nonlinear interpolation technique to cope with missing data points, J. Geophys. Res., 106, 30077–30083, doi:10.1029/2000JA002227, 2001.

Hanbaba, R.: Improved quality of services ionospheric telecommunication systems planning and operation, Cost Action 251, Final Report, Published by Space Research Centre, Warsaw, Poland, 1999.

IPS-Radio and Space Services: ASAPS V6, available at http://www.ips.gov.au/Products_and_Services/1/1, undated, last accessed May 2013.

Koutroumbas, K., Tsagouri, I., and Belehaki, A.: Time series autoregression technique implemented on-line in DIAS system for ionospheric forecast over Europe, Ann. Geophys., 26, 371–386, doi:10.5194/angeo-26-371-2008, 2008.

Liu, R., Xu, Z., Wu, J. S., Liu, Zhang, B., and Wang, G.: Preliminary studies on ionospheric forecasting in China and its surrounding area, J. Atmos. Sol. Terr. Phys., 67, 1129–1136, doi:10.1016/j.jastp.2004.12.012, 2005.

Mikhailov, A. V., De la Morena, B. A., Miro, G., and Marin, D.: A method for *fo*F2 monitoring over Spain using the EI Arenosillo Digisonde current observations, Ann. Geophys., 42, 683–689, 1999.

Muhtarov, P. and Kutiev, I.: Autocorrelation method for temporal interpolation and short-term prediction of ionospheric data, Radio Sci., 34, 459–464, 1999.

Oyeyemi, E. O., Poole, A. W. V., and McKinnell, L. A.: On the global short-term forecasting of the ionospheric critical frequency *fo*F2 up to 5 hours in advance using neural networks, Radio Sci., 40, RS6012, doi:10.1029/2004RS003239, 2005.

Perrone, L., De Franceschi, G., and Gulyaeva, T. L.: The time-weighted magnetic indices ap(τ), PC(τ), AE(τ) and their correlation to the southern high latitude ionosphere, Phys. Chem. Earth (C), 26, 331–334, 2001.

Pezzopane, M., Pietrella, M., Pignatelli, A., Zolesi, B., and Cander, Lj. R.: Assimilation of autoscaled data and regional and local ionospheric models as input sources for a real-time 3-D International Reference Ionosphere modelling, Radio Sci., 46, RS5009, doi:10.1029/2011RS004697, 2011.

Pezzopane, M., Pietrella, M., Pignatelli, A., Zolesi, B., and Cander, Lj. R.: Testing the three-dimensional IRI-SIRMUP-P mapping of the ionosphere for disturbed periods, Adv. Space Res., online first, doi:10.1016/j.asr.2012.11.028, 2013.

Pietrella, M.: A short-term ionospheric forecasting empirical regional model (IFERM) to predict the critical frequency of the F2 layer during moderate, disturbed, and very disturbed geomagnetic conditions over the European area, Ann. Geophys., 30, 343–355, doi:10.5194/angeo-30-343-2012, 2012.

Pietrella, M. and Perrone, L.: Instantaneous Space Weighted Ionospheric Regional Model for instantaneous mapping of the critical frequency of the F2 layer in the European region, Radio Sci., 40, RS1005, doi:10.1029/2003RS003008, 2005.

Pietrella, M. and Perrone, L.: A local ionospheric model for forecasting the critical frequency of the F2 layer during disturbed geomagnetic and ionospheric conditions, Ann. Geophys., 26, 323–334, doi:10.5194/angeo-26-323-2008, 2008.

Pietrella, M., Perrone, L., Fontana, G., Romano, V., Malagnini, A., Tutone, G., Zolesi, B., Cander, Lj. R., Belehaki, A., Tsagouri, I., Kouris, S. S., Vallianatos, F., Makris, J. P., and Angling, M.: Oblique-incidence ionospheric soundings over Central Europe and their application for testing now casting and long term prediction models, Adv. Space Res., 43, 1611–1620, 2009.

Radicella, S. M.: The NeQuick model genesis, uses and evolution, Ann. Geophys., 52, 417–422, 2009.

Settimi, A., Pezzopane, M., Pietrella, M., Bianchi, C., Scotto, C., Zuccheretti, E., and Makris, J.: Testing the IONORT-ISP system: A comparison between synthesized and measured oblique ionograms, Radio Sci., 48, 167–179, doi:10.1002/rds.20018, 2013.

Stanislawska, I. and Zbyszynski, Z.: Forecasting of ionospheric characteristics during quiet and disturbed conditions, Ann. Geophys., 45, 169–175, 2002.

Stewart, F. G.: ICEPAC-Technical Manual, available at http://www.greg-hand.com/manuals/icepac_tech_manual.pdf, undated, last access date May 2013.

Strangeways, H. J., Kutiev, I., Cander, Lj. R., Kouris, S., Gherm, V., Marin, D., De La Morena, B. A., Pryse, S. E., Perrone, L., Pietrella, M., Stankov, S., Tomasik, L., Tulunay, E., Tulunay, Y., Zernov, N., and Zolesi, B.: Near-Earth space plasma modelling and forecasting, Ann. Geophys., 52, 255–271, 2009.

Tsagouri, I., Zolesi, B., Belehaki, A., and Cander, L. R.: Evaluation of the performance of the real time updated simplified ionospheric regional model for the European area, J. Atmos. Sol. Terr. Phys., 67, 1137–1146, doi:10.1016/j.jastp.2005.01.012, 2005.

Wrenn, G. L.: Time-Weighted accumulations ap(τ) and Kp(τ), J. Geophys. Res., 92, 10125–10129, 1987.

Wrenn, G. L., Rodger, A. S., and Rishbeth, H.: Geomagnetic storms in Antarctic F region. I. Diurnal and seasonal patterns in main phase effects, J. Atmos. Terr. Phys., 49, 901–913, 1987.

Zolesi, B., Cander, Lj. R., and De Franceschi, G.: Simplified ionospheric regional model (SIRM) for telecommunications applications, Radio. Sci., 4, 603–612, 1993.

Zolesi, B., Cander, Lj. R., and De Franceschi, G.: On the potential applicability of the simplified ionospheric regional model to different midlatitude areas, Radio Sci., 31, 547–552, doi:10.1029/95RS03817, 1996.

Zolesi, B., Belehaki, A., Tsagouri, I., and Cander, Lj. R.: Real-time updating of the Simplified Ionospheric Regional Model for operational applications, Radio Sci., 39, RS2011, doi:10.1029/2003RS002936, 2004.

Zolesi, B., Fontana, G., Perrone, L., Pietrella, M., Romano, V., Tutone, G., Belehaki, A., Tsagouri, I., Kouris, S. S., Vallianatos, F., Makris, J. P., and Angling, M. J.: A new campaign for oblique-incidence ionospheric sounding over Europe and its data application, J. Atmos. Terr. Phys., 70, 854–865, 2008.